

Screening-Engineered Field-Effect Solar Cells

William Regan,^{†,‡,||} Steven Byrnes,^{†,‡,||} Will Gannett,^{†,‡} Onur Ergen,^{†,‡,§} Oscar Vazquez-Mena,^{†,‡} Feng Wang,^{†,‡,§} and Alex Zettl^{*,†,‡,§}

[†]Department of Physics, University of California at Berkeley, Berkeley, California 94720, United States

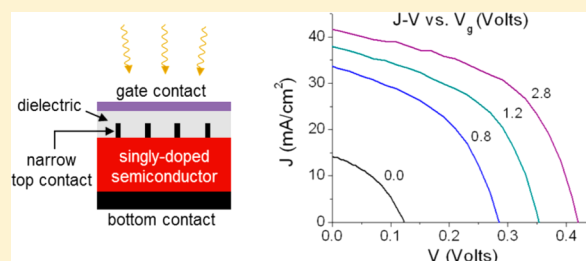
[‡]Materials Sciences Division, Lawrence Berkeley National Laboratory, Berkeley, California 94720, United States

[§]Center of Integrated Nanomechanical Systems, University of California at Berkeley, Berkeley, California 94720, United States

Supporting Information

ABSTRACT: Photovoltaics (PV) are a promising source of clean renewable energy, but current technologies face a cost-to-efficiency trade-off that has slowed widespread implementation.^{1,2} We have developed a PV architecture—screening-engineered field-effect photovoltaics (SFPV)—that in principle enables fabrication of low-cost, high efficiency PV from virtually any semiconductor, including the promising but hard-to-dope metal oxides, sulfides, and phosphides.³ Prototype SFPV devices have been constructed and are found to operate successfully in accord with model predictions.

KEYWORDS: Photovoltaics, earth abundant semiconductors, electric field effect, Schottky barriers



Screening-engineered field-effect photovoltaics (SFPV) uses the well-understood electric field effect, enabled via a carefully designed partially screening top electrode, to tune the electrode-semiconductor junction. The application of the field effect to PV dates back nearly four decades to metal-insulator-semiconductor (MIS) cells, in which a thin insulating layer is used to block the recombination current. Such cells typically employ fixed, uncompensated charges (functioning like a gate) with a dielectric coating to increase the semiconductor band bending at the MIS interface. Unfortunately, MIS cells, though sporting impressive efficiencies,^{4–6} typically have short operating lifetimes due to surface state instability at the MIS interface.⁷ Methods aimed at direct field-effect “doping” of semiconductors, in which the voltage is externally applied to a gate to invert a region of semiconductor,^{5,6,8,9} have been ultimately limited by screening of the gate near the top contact. To be effective, such gating methods must rely on other cumbersome strategies in addition to the gate, such as doping under the top contacts^{8,9} or having a large Schottky barrier at the top contacts.^{4–6} Recent encouraging efforts to overcome this limitation have targeted low density-of-states Schottky contacts.^{10–12}

In the present work, we solve generally the fundamental problem of screening and show how a stable, electrically contacted p–n junction can be achieved with nearly any semiconductor and any electrode material (even ohmic contacts) through the application of a gate field, provided that the electrode is geometrically structured appropriately. The gating method can be applied to semiconductor materials heretofore deemed unsuitable for PV, as well as to currently used materials and architectures in an enhancement mode. We also present a self-gating configuration, where the gate is sustained “internally” by electrical activity of the cell itself,

eliminating the need for an external gate power source and thus simplifying practical SFPV device implementation.

The key to effective field-effect implementation in PV is “minimal screening,” whereby the action of a gate and the current-carrying cell electrode (i.e., top contact) beneath it allow for simultaneous electrical contact to and carrier modulation of the top surface of the semiconductor. This can be achieved by restricting at least one dimension of the top contact, for example by shaping the contact into narrow fingers (type A) or by making the top contact uniformly very thin (type B), as shown schematically in Figure 1 parts a and d, respectively. In type A devices, sufficiently narrow fingers allow the gate field to create a low resistance inversion layer between fingers and deplete the semiconductor beneath the fingers, resulting in a p–n junction and pinching off the shunt path through the semiconductor. In type B devices, the out-of-plane thickness of the top contact is chosen to be thinner than its Debye screening length, to allow electric fields to penetrate and deplete/invert the underlying semiconductor. In both configurations, the gate dielectric can conveniently serve a dual role and function also as an antireflection coating (not further considered here).

We now consider theoretically details of these configurations. We evaluate type A, or “nanofinger,” electrodes using finite-element simulations (see Supporting Information). The inputs to the model are semiconductor type (chemical doping type and carrier concentration N_D), total wafer thickness D , depletion width d , thickness t and dielectric constant κ of the gate dielectric, and work function ϕ and geometry (width w and

Received: May 27, 2012

Revised: July 6, 2012

Published: July 16, 2012

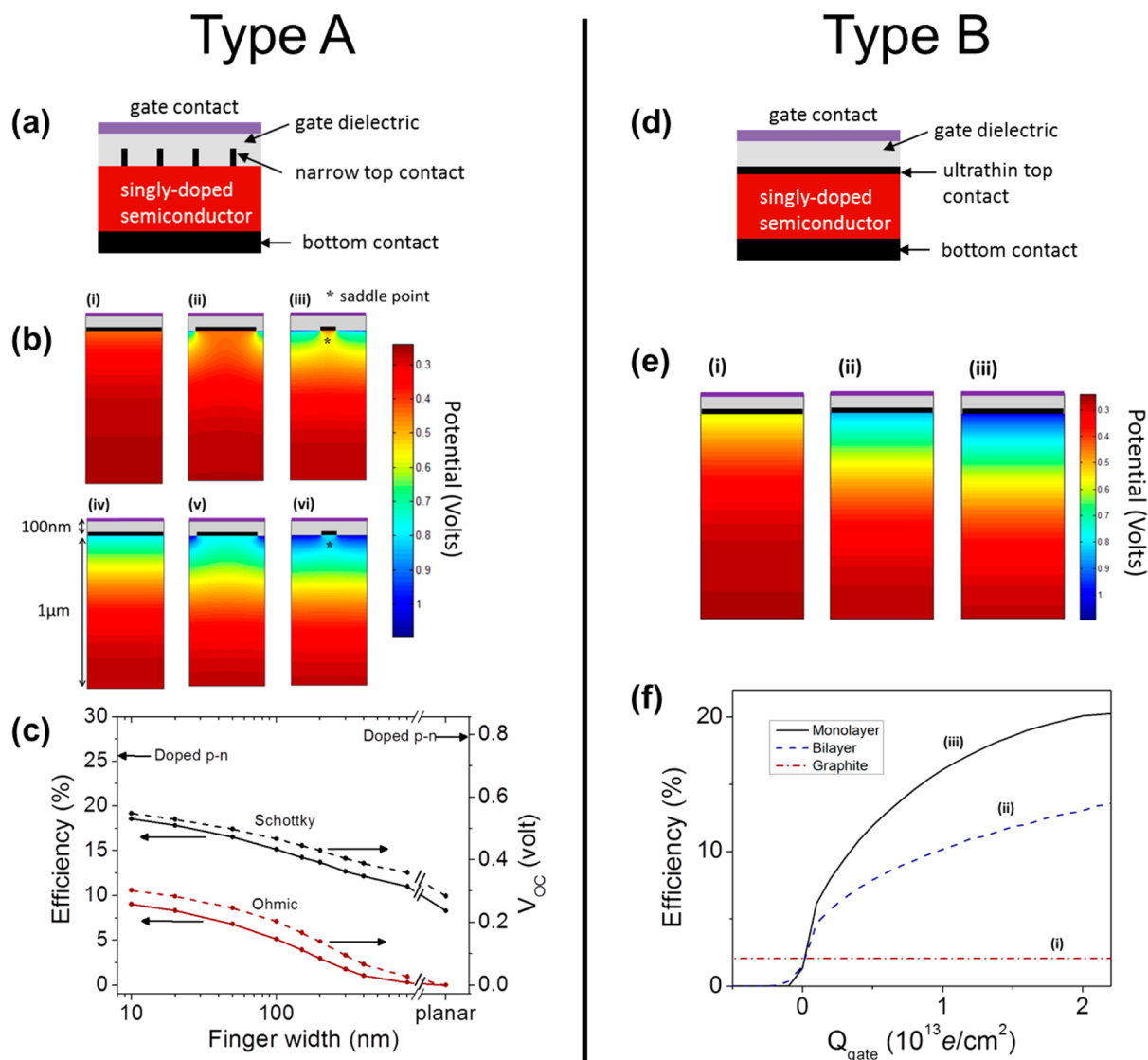


Figure 1. Simulations for SFPV cells. (a) Schematic of type A cell. (b) Potential plots for various finger widths w (planar, 400 nm, 100 nm) for ohmic (i–iii) and Schottky (iv–vi) contacts to n-type Si ($N_D = 10^{15}/\text{cm}^3$) with saturated gate ($V_g = -10$ V). (c) Efficiency and V_{oc} for ohmic and Schottky contacts as a function of w . (d) Schematic of type B cell. (e) Potential plots for graphite, bilayer graphene, and monolayer graphene (i–iii) on n-type Si ($N_D = 10^{15}/\text{cm}^3$) with saturated gate ($Q_{\text{gate}} = 1.5 \times 10^{13} \text{ e}/\text{cm}^2$). (f) Efficiency for graphite, bilayer graphene, and monolayer graphene as a function of gate charge.

center-to-center separation s) of the fingers. We limit our theoretical analysis to metal nanofingers in direct contact with the semiconductor, but the SFPV geometry can be utilized with semimetal or semiconductor nanofingers, either in direct contact with the semiconductor or in an MIS or semiconductor–insulator–semiconductor (SIS) configuration. In Figure 1b and c we show results using inputs typical for the prototype materials Si and SiO_2 : n-type Si, $D = 10 \mu\text{m}$, $N_D = 10^{15}/\text{cm}^3$, $d = 1 \mu\text{m}$, $t = 100 \text{ nm}$, $\kappa = 3.9$, $\phi = 4.45 \text{ eV}$ (ohmic) or $\phi = 4.8 \text{ eV}$ (Schottky), $s = 10 \mu\text{m}$, and variable finger width w . Changing the wafer doping a few orders of magnitude above or below this middle-range level only changes the scaling of the simulation. Considerations of changing the finger separation are discussed in the Supporting Information (Figure S1).

Figure 1b shows a simulation of potential profiles for screening through wide and narrow finger contacts: planar ($w = \infty$), $w = 400 \text{ nm}$, and $w = 100 \text{ nm}$, for both ohmic (i–iii) and Schottky (iv–vi) contacts. The finger contacts are held at ground, and the gate is held at -10 V for all simulations shown,

which produces a sufficiently large field for the effect to saturate and makes the choice of gate metal (specifically, its work function) unimportant. Wide fingers screen out all effects of the gate underneath themselves, and the resulting shunt current path dominates the transport. However, with sufficiently narrow fingers (Figure 1b iii and vi), the gate field can spread under the electrode, creating a potential profile with a saddle point under the electrode. To travel from the bottom to the top electrode, majority carriers must climb over the saddle point, which forms a larger barrier than the intrinsic Schottky barrier, thereby directly lowering the diode saturation current and improving the solar cell performance. Simulated current–voltage (IV) curves for these cells are found in the Supporting Information (Figure S2).

Attainable open circuit voltage and efficiency increase considerably with decreasing finger width w , as seen in Figure 1c. The observed improvement far exceeds that expected from reduced contact areas alone.¹³ As this example shows, the electrode finger size is a primary factor controlling the size and

presence of a saddle-point potential barrier. For the effect to be strong, the finger width must be much smaller than the depletion width in the semiconductor, as this is the length scale over which the potential varies in the semiconductor. Additional factors affecting the saddle-point barrier are bias, with forward bias advantageously raising the barrier, and the intrinsic Schottky barrier.

We next consider type B cells (Figures 1d–f) in which the partially screening top contact is an ultrathin metallic or semimetallic sheet of uniform thickness. In our theoretical analysis the electronic properties of the sheet material are critical. For a practical device graphene is an attractive choice; hence for our simulations we input graphene (mono-, bi-, or multi-layer) as the ultrathin contact. Graphene is highly transparent ($\sim 97.7\%$ /layer) yet reasonably conductive,¹⁴ forms a Schottky contact to n- and p-type Si,^{15,16} and has a low density-of-states near the charge neutral point, allowing electric fields to partially penetrate one or more layers and tune the graphene work function.¹⁷ Thus, graphene can act as a continuous, transparent top electrode but still allow electric fields to penetrate and deplete/invert the underlying semiconductor. Details of simulations of our type B graphene devices can be found in the Supporting Information.

Simulated potential profiles (with a saturated gate) as a function of depth into a prototype semiconductor (n-type Si, donor concentration $N_D = 10^{15}/\text{cm}^3$) for monolayer, bilayer, and multi-layer graphene are shown in Figure 1e. In Figure 1f, the predicted overall cell efficiency as a function of negative gate charge is shown for the same graphene-based top contacts; plots of Schottky barrier height versus gate charge for these cells are found in the Supporting Information (Figure S3). As expected monolayer graphene performs best, achieving power conversion efficiency up to $\sim 19\%$, since it permits the most field penetration. We note that the simulation does not consider the possible limiting effect of the high sheet resistance of monolayer graphene, since this could be easily mitigated via a mesh of attached metal busbars or other modifications.^{18–21}

We now turn to SFPV experimental device fabrication and characterization. Guided by our model predictions, both type A and type B cells are successfully realized. To distinguish the SFPV effect from improvements due solely to surface passivation, we fabricate type A SFPV cells with intrinsically ohmic (annealed Al) nanofinger contacts on $N_A \sim 1 \times 10^{16}/\text{cm}^3$ p-type Si; a schematic of this device is shown in the inset of Figure 2. We use 250 nm wide contacts—a bit less than the Si depletion width (similar to cell ii in Figure 1b)—with a 5 μm lateral spacing. A top gate is formed with an additional 150 nm of electron-beam evaporated SiO_2 and a semitransparent ($\sim 40\%$) Cr/Au gate contact. A series of IV plots (AM1.5 illumination) as a function of gate voltage (V_g) is shown in Figure 2.

During device testing, the nanofingers are held at ground, and V_g is fixed, while the bias voltage (bottom contact) is varied. A positive V_g repels holes in the top layer of the p-type Si and pulls in electrons through the fingers. Increasing the positive V_g tunes the initially ohmic contact (at $V_g = 0.0$ V) into a Schottky contact, monotonically increasing open circuit voltage (V_{oc}), short circuit current (I_{sc}), fill factor (FF), and shunt resistance (R_{shunt}). The power conversion efficiency (PCE) and V_{oc} are $\sim 1.4\%$ (see Supporting Information for refinements based on cell area) and 0.09 V at $V_g = 3.2$ V, respectively, near theoretical expectations. Once established, the gate field takes negligible power to maintain; at $V_g = 3.2$ V,

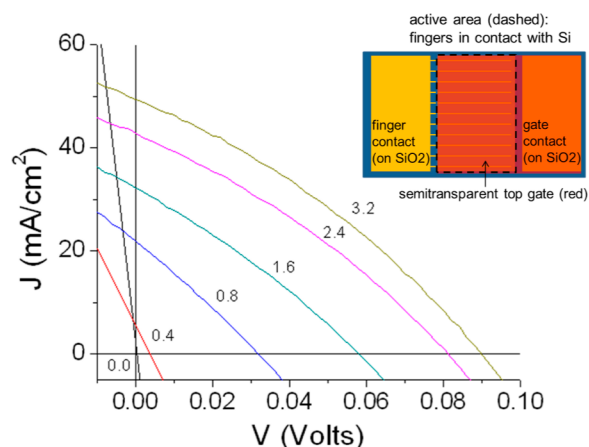


Figure 2. Experimental IV plots for type A SFPV with ohmic nanofinger contacts to p-type Si. Positive V_g (curve labels in Volts) transforms ohmic Al contacts into rectifying contacts. Power conversion efficiency at $V_g = 3.2$ V is $\sim 1.4\%$ (see Supporting Information for refinements based on cell area) with a negligible steady state gate current (6.6 nA). A schematic of the device is seen in the inset. The p-type Si ($N_A \sim 1 \times 10^{16}/\text{cm}^3$) is contacted with 250 nm wide annealed Al fingers, and the gate is composed of 150 nm SiO_2 and a $\sim 40\%$ transparent Cr/Au film. Contact pads rest on 100 nm thermally grown SiO_2 . Illumination is AM1.5.

the steady state gate current I_g is only 6 nA, many orders of magnitude below I_{sc} . In this example, the steady state gate power consumption ($P_g = V_g I_g$) at $V_g = 3.2$ V is approximately 3 orders of magnitude smaller than the photovoltaic power generated at the maximum power point, demonstrating the feasibility of this technique for practical devices. We note that several parameters may yet be optimized, such as gate transparency, gate thickness, dielectric quality, finger spacing and width, antireflection coating effectiveness, and surface texturing.

Much higher cell efficiencies can be attained by starting with Schottky contacts. Experimental results for type A cells with intrinsically Schottky (Cr on p-type Si) contacts can be found in the Supporting Information (Figures S4a and S4b). Similar improvements in V_{oc} , I_{sc} , FF, and PCE are demonstrated, again consistent with theoretical predictions. We additionally show that this effect can be reversed—that an initially Schottky contact can be made ohmic—by gating with the opposite polarity. This symmetry may present compelling opportunities for improving nonideal ohmic contacts.

To demonstrate the universality of the SFPV effect, we created type A cells using Cu_2O , a hard-to-dope, earth-abundant semiconductor with great potential for low-cost PV cells.²² Cu_2O foils are grown using thermal oxidation²² and mechanically polished. A SFPV heterojunction is created with ITO nanofingers (750 nm wide with 5 μm spacing) contacting the p-type Cu_2O and a top gate comprised of ITO on a MgO dielectric. As seen in Figure 3, the application of a small V_g (20 mV) yields an enhancement factor of nearly 1.6 in PCE. When applied to optimized devices, the SFPV architecture may enable much higher efficiencies than present world records and make Cu_2O and related materials practical for commercial PV cells.

We fabricate type B cells using chemical vapor deposition (CVD) grown graphene as the ultrathin top contact. Monolayer graphene is brought in contact with n-type Si ($N_D \sim 10^{16}/\text{cm}^3$) and is contacted with evaporated Cr/Au. A gate field is applied using ionic liquid (EMI-BTI, Sigma Aldrich No.

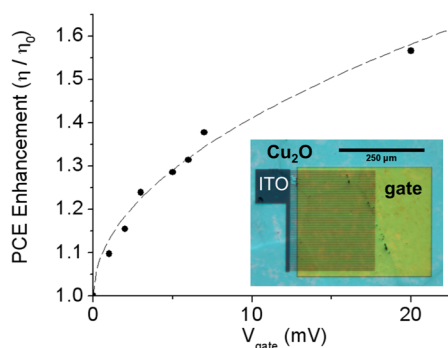


Figure 3. Experimental IV plots for type A SFPV with Schottky contacts to Cu_2O absorber. A small V_g increases power conversion efficiency (PCE) by a factor of nearly 1.6, demonstrating the universality of the SFPV effect. The dashed line is a guide to the eye. As seen in the optical micrograph (inset), ITO nanofingers (750 nm wide, 5 μm spacing) make contact to the p-type Cu_2O , and gating is accomplished with an ITO contact and a MgO dielectric. Illumination is AM1.5.

11291). A series of experimental IV plots as a function of V_g is shown in Figure 4, with an optical micrograph of the device shown as an inset.

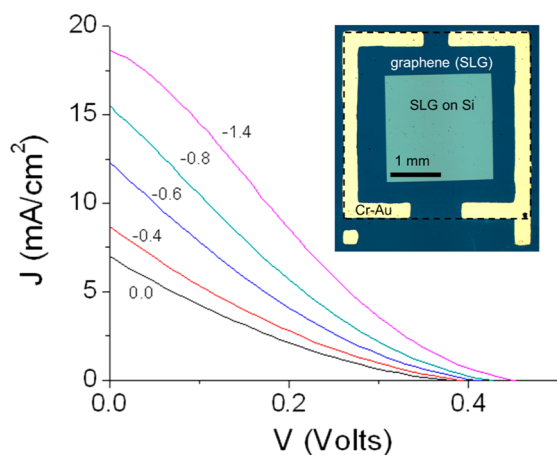


Figure 4. Experimental IV plots for type B SFPV with graphene contact to n-type Si. As seen in the optical micrograph (inset), single layer (SLG) graphene is applied to n-type Si ($N_D \sim 10^{16}/\text{cm}^3$). The Cr/Au contact to graphene rests on 100 nm SiO_2 . V_{oc} , I_{sc} , and FF increase appreciably with negative gating. Power conversion efficiency rises from $\sim 0.5\%$ ($V_g = 0.0$ V) to $\sim 1.8\%$ ($V_g = -1.4$ V). Illumination is AM1.5, and gating (curve labels in Volts) is achieved with an ionic liquid (EMI-BTI).

To test the type B device, the graphene is held at ground, and the gate is held at a fixed voltage, while the bias voltage (bottom contact) is varied. A negative V_g repels electrons in the top layer of the n-type Si and graphene. A modest V_g (with negligible gate power) notably enhances V_{oc} , I_{sc} , and the FF, increasing PCE from $\sim 0.5\%$ with $V_g = 0.0$ V to $\sim 1.8\%$ with $V_g = 1.2$ V. Similar results for “bilayer” graphene (via transferring an additional monolayer) can be found in the Supporting Information (Figure S5).

While the power consumed by the gate for SFPV devices can be negligible, the requirement of an external gate power source applied to a third lead could increase the complexity and cost of a commercial SFPV device. Additionally, when connecting SFPV modules in series to boost the module voltage, the

ground of all but the initial cell must be floated and increased in steps of the cell operating voltage. As a result, the gate at subsequent cells must also increase in steps of the cell voltage. To address these issues, we propose a simple modification: by connecting the cell output to the gate, the gate can be self-powered, with an appropriately floated ground. Self-gating can lead to a feedback loop which notably increases the cell output, given appropriate choices of gate metal (with a large work function for n-type semiconductors or a small work function for p-type), gate dielectric material and thickness, and porous top electrode (which should form some initial Schottky contact or heterojunction which the gate can further enhance). We repeat our previous simulations for an appropriately chosen gate metal and a thin gate dielectric (see Supporting Information, Figure S6) and find that self-gating is indeed able to attain nearly the same ultimate efficiency as with a saturated, externally powered gate. We note that this effective gating may also be applied through the use of dielectrics, electrolytes, ferroelectrics, or other materials with fixed bulk or surface charges at the interface with the semiconductor.^{23,24} Additionally, these two strategies (a self-gating feedback loop and gate materials with fixed or surface charges) may be used in tandem to provide a more pronounced gating effect.

Using one of our prototypes, a type A SFPV with 250 nm wide Schottky (Cr) contacts to $N_A = 3 \times 10^{15}$ p-type Si and an EMI-BTI ionic liquid gate, we experimentally demonstrate self-gating. The cell is placed under AM1.5 illumination with the fingers and gate initially held at ground. In Figure 5, we plot V_{oc}

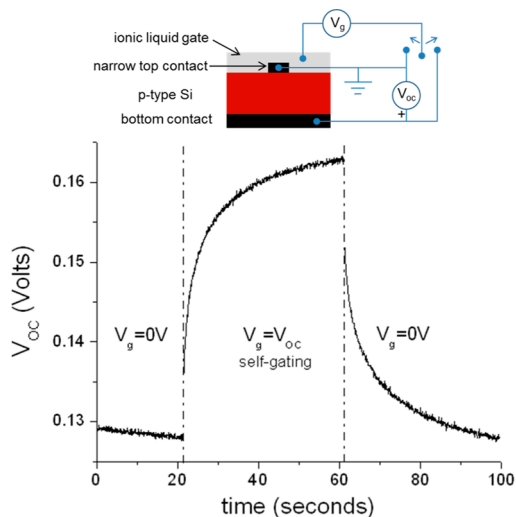


Figure 5. Self-gating of type A SFPV. A demonstration of the self-gating effect using a type A device: 250 nm wide Cr Schottky nanofinger contacts to p-type Si ($N_A = 3 \times 10^{15}/\text{cm}^3$). Illumination is AM1.5, and gating is achieved with an ionic liquid (EMI-BTI). With the nanofingers held at ground, the gate is toggled between ground and V_{oc} (the bottom ohmic contact), and V_{oc} is plotted versus time. A 30% relative increase in V_{oc} is seen while in the self-gating configuration, corresponding to a $\sim 60\%$ relative increase in power conversion efficiency.

versus time while the gate is toggled between ground and the cell output (bottom electrode). We observe a large increase in V_{oc} (30%) over the nongated Schottky barrier configuration and a $\sim 60\%$ increase in PCE. Successful self-gating is thus demonstrated.

In conclusion, through careful control of the screening properties of the top electrodes, a general method is developed to predict and produce high quality, field-induced semiconductor p–n junctions. This architecture offers the benefits of previously demonstrated MIS and field-induced junctions—energy savings in fabrication and no doping-related crystal damage—and also relaxes the limitation of top contact Schottky barrier heights. This flexibility should allow many previously inaccessible p–n junctions to be constructed, such as those using difficult-to-dope compound semiconductors that may hold the key to making solar energy an affordable, primary energy source.

■ ASSOCIATED CONTENT

Supporting Information

Supporting methods and discussion and Figures S1–S6. This material is available free of charge via the Internet at <http://pubs.acs.org>.

■ AUTHOR INFORMATION

Corresponding Author

*E-mail: azettl@berkeley.edu.

Author Contributions

^{||}These authors contributed equally.

Notes

The authors declare no competing financial interest.

■ ACKNOWLEDGMENTS

This research was supported in part by the Director, Office of Energy Research, Materials Sciences and Engineering Division, of the U.S. Department of Energy under Contract No. DE-AC02-05CH11231 which provided for theoretical analysis, design of the experiment, and characterization of the cells; by the National Science Foundation within the Center of Integrated Nanomechanical Systems, under Grant EEC-0832819, which provided for Cu₂O synthesis; and by the Office of Naval Research (MURI) which provided for graphene synthesis and assembly. F.W. and S.B. acknowledge support through a Department of Energy Early Career Award, DE-SC0003949. W.R. and S.B. acknowledge support through a National Science Foundation Graduate Research Fellowship, and O.V. acknowledges support by the Swiss National Science Foundation (SNSF). W.R., S.B., F.W., and A.Z. conceived the SFPV device structures, and W.R. and A.Z. conceived the self-gating configuration; S.B. performed all simulations; W.R. fabricated and tested all devices, with assistance from W.G., O.E., and O.V.; W.R., S.B., and A.Z. wrote the paper. All authors discussed the results and commented on the manuscript.

■ REFERENCES

- (1) Razykov, T. M.; Ferekides, C. S.; Morel, D.; Stefanakos, E.; Ullal, H. S.; Upadhyaya, H. M. *Sol. Energy* **2011**, *85* (8), 1580–1608.
- (2) Wolden, C. A.; Kurtin, J.; Baxter, J. B.; Repins, I.; Shaheen, S. E.; Torvik, J. T.; Rockett, A. A.; Fthenakis, V. M.; Aydil, E. S. *J. Vac. Sci. Technol. A* **2011**, *29* (3), 030801.
- (3) Wadia, C.; Alivisatos, A. P.; Kammen, D. M. *Environ. Sci. Technol.* **2009**, *43* (6), 2072–2077.
- (4) Green, M. A.; King, F. D.; Shewchun, J. *Solid-State Electron.* **1974**, *17* (6), 551–561.
- (5) Yeh, D. K.; Demassa, T. A. *Solid-State Electron.* **1984**, *27* (3), 283–292.

- (6) Yerokhov, V. Y.; Melnyk, I. I. *Solid-State Electron.* **1998**, *42* (6), 883–889.
- (7) Gomaa, N. G. *Renewable Energy* **2001**, *24* (3–4), 529–534.
- (8) Fujioka, H.; Oshima, M.; Hu, C.; Sumiya, M.; Matsuki, N.; Miyazaki, K.; Koinuma, H. *J. Non-Cryst. Solids* **1998**, *227*, 1287–1290.
- (9) De Cesare, G.; Chicarella, E.; Palma, E.; Nobile, G.; Tucci, M. *Thin Solid Films* **2003**, *427* (1–2), 166–170.
- (10) Liu, B.; McCarthy, M. A.; Yoon, Y.; Kim, D. Y.; Wu, Z. C.; So, F.; Holloway, P. H.; Reynolds, J. R.; Guo, J.; Rinzler, A. G. *Adv. Mater.* **2008**, *20* (19), 3605–3609.
- (11) Wadhwa, P.; Liu, B.; McCarthy, M. A.; Wu, Z. C.; Rinzler, A. G. *Nano Lett.* **2010**, *10* (12), 5001–5005.
- (12) Wadhwa, P.; Seol, G.; Petterson, M. K.; Guo, J.; Rinzler, A. G. *Nano Lett.* **2011**, *11* (6), 2419–2423.
- (13) Green, M. A. *Appl. Phys. Lett.* **1975**, *27* (5), 287–288.
- (14) Nair, R. R.; Blake, P.; Grigorenko, A. N.; Novoselov, K. S.; Booth, T. J.; Stauber, T.; Peres, N. M. R.; Geim, A. K. *Science* **2008**, *320* (5881), 1308–1308.
- (15) Li, X. M.; Zhu, H. W.; Wang, K. L.; Cao, A. Y.; Wei, J. Q.; Li, C. Y.; Jia, Y.; Li, Z.; Li, X.; Wu, D. H. *Adv. Mater.* **2010**, *22* (25), 2743–2748.
- (16) Chen, C. C.; Aykol, M.; Chang, C. C.; Levi, A. F. J.; Cronin, S. B. *Nano Lett.* **2011**, *11* (5), 1863–1867.
- (17) Cox, M.; Gorodetsky, A.; Kim, B.; Kim, K. S.; Jia, Z.; Kim, P.; Nuckolls, C.; Kymissis, I. *Appl. Phys. Lett.* **2011**, *98* (12), 123303(1–3).
- (18) Zhu, Y.; Sun, Z. Z.; Yan, Z.; Jin, Z.; Tour, J. M. *ACS Nano* **2011**, *5* (8), 6472–6479.
- (19) Tung, V. C.; Chen, L. M.; Allen, M. J.; Wassei, J. K.; Nelson, K.; Kaner, R. B.; Yang, Y. *Nano Lett.* **2009**, *9* (5), 1949–1955.
- (20) Shi, Y. M.; Kim, K. K.; Reina, A.; Hofmann, M.; Li, L. J.; Kong, J. *ACS Nano* **2010**, *4* (5), 2689–2694.
- (21) Liu, J. W.; Xu, G. W.; Rochford, C.; Lu, R. T.; Wu, J.; Edwards, C. M.; Berrie, C. L.; Chen, Z. J.; Maroni, V. A. *Appl. Phys. Lett.* **2011**, *99* (2), 023111(1–3).
- (22) Mittiga, A.; Salza, E.; Sarto, F.; Tucci, M.; Vasanthi, R. *Appl. Phys. Lett.* **2006**, *88* (16), 163502(1–2).
- (23) Hiremath, R. K.; Rabinal, M. K.; Mulimani, B. G.; Khazi, I. M. *Langmuir* **2008**, *24* (19), 11300–11306.
- (24) Hsu, W.-W.; Chen, J. Y.; Cheng, T.-H.; Lu, S. C.; Ho, W.-S.; Chen, Y.-Y.; Chien, Y.-J.; Liu, C. W. *Appl. Phys. Lett.* **2012**, *100* (2), 023508(1–3).